On the use of rock physics models for studying the critical zone

Vanshan Wright[1,2*] and Matthew Hornbach[1]

[1]Southern Methodist University, Roy Huffington Department of Earth Sciences, Dallas, Texas, 75275-0395.

[2]Woods Hole Oceanographic Institution, Department of Geology and Geophysics, Woods Hole, Massachusetts, 02543

*now at

Corresponding author: Vanshan Wright (vwright@whoi.edu)

Key Points:

- Rock physics model performance depends on sediment age
- Jenkins, followed by Walton, and Hertz-Mindlin models perform best in cementless critical zone sands
- Rock physics models remain non-unique primarily because of a lack of constraint on how grain-contact forces are distributed in sands

ABSTRACT

How effective are rock physics models for relating seismic velocities to the physical properties of sediments, fluids, and cement within the critical zone, and what factors most substantially influence the models' accuracies? We answer these questions by testing and analyzing the accuracies of seven rock physics models (Hertz-Mindlin, Walton, Jenkins, Digby, stiff sand, soft sand, and contact cement) for estimating seismic velocities of vadose zone sands at Port Royal Beach in Jamaica. These sands are clean, well-rounded, and highly-spherical, which are ideal for rock physics model testing. Measured velocities and model input parameters (e.g., porosity, density, grain size, and fluid saturation percentage) derive from seismic refraction surveys and sidewall sediment cores, respectively. We find that, in their current forms, all seven rock physics models overpredict seismic velocities for sands deposited within the last forty-three years. Misfits between measured and predicted velocities reduce with time since deposition, with all but one (Digby) cementless models accurately predicting the seismic velocities for sands older than ninety-five years. Jenkins, followed by Walton, Hertz-Mindlin, and soft sand models are generally most accurate (i.e., have the lowest misfits), possibly because high porosity sands are more susceptible to tangential slip during seismic wave propagation. We conclude that the models will most substantially improve when the effects of the existence and locations of strong versus weak force-chain links are included in their respective equations.

1 Introduction

The critical zone is the shallow section of the earth's crust, where living organisms, porous sediments, and fluids interact. There is an ongoing need to understand this section of earth's crust better, partly because of its importance for combatting the adverse effects of climate change as well as its role in water conservation (e.g., Anderson et al., 2007; Parsekian et al., 2015). Researchers often characterize the critical zone using above-ground geophysical surveys, which can be cheaper and more feasible than direct sampling methods such as drilling (Parsekian et al., 2015). Common surface-based geophysical studies include electromagnetic, ground-penetrating radar, nuclear magnetic resonance, electrical resistivity, magnetotelluric, and seismic refraction surveys (e.g., Selker et al., 2006; Rodell et al., 2007; Rabbel, 2010). Measured geophysical observables from these surveys (e.g., seismic velocities) are often integrated with empirical and theoretical models (e.g., empirical porosity-velocity curves and rock physics models) to provide quantitative links between the surveyed properties (e.g., seismic velocities) and the physical properties of buried sediments and fluids (Day-Lewis et al., 2005; Parsekian et al., 2015). Studying the critical zone in this way relies on the accuracy of empirical and theoretical models.

The integration of seismic velocities and rock physics models represents a promising method for constraining critical zone sediments, fluids, grain microstructure, and cement (Holbrook et al., 2014; Shen et al., 2016; Flinchum et al., 2018). Methods for deriving seismic velocities from refraction surveys (e.g., first-break geometric, tau-p, and seismic tomography) are well-known and reasonably advanced but sometimes produce inconsistent results owing to variations in first-arrival picks, velocity averaging, and/or tradeoffs between velocity and layer thickness, and the inherent non-uniqueness in the geophysical inverse methods used to constrain velocity profiles (e.g., Mota, 1954; Stephenson et al., 2005). Rock physics models predict seismic velocities by integrating estimates for porosity, bulk density, grain size, coordination number, effective pressure, cement fraction, grain friction, and mineral Poisson's ratio (Mavko et al., 2020). Their use in critical zone studies remains contentious primarily because (1) the models produce non-unique solutions due to a large number of variables, (2) model constraints often lack ground-truthing in the critical zone that reduces model uncertainty, and (3) different models use different physical approaches or assumptions to estimate seismic velocity (Day-Lewis et al., 2005). An open question is whether improvements to the models are needed before they are widely used in the critical zone.

The seven most commonly used rock physics models are Hertz-Mindlin, Digby, Walton, Jenkins, contact cement, stiff sand, and soft sand (Mindlin, 1949; Digby, 1981; Walton, 1987; Dvorkin & Nur, 1996; Jenkins et al., 2005; Mavko et al., 2020). Hertz-Mindlin is the only model that has been tested in multiple deep-marine and shallow critical zone sands (Bachrach et al., 2000; Bachrach & Avseth, 2008; Andersen & Johansen, 2010). Hertz-Mindlin performs best for compressional wave velocities *Vp* in deep-buried (>400 km) sands but overpredicts shear wave velocities *Vs* at similar depths (Bachrach et al., 2000; Andersen & Johansson, 2010). Specifically, Hertz-Mindlin overpredicts *Vp* and *Vs* in vadose zone sands, assuming average sand properties (Bachrach et al., 2000; Andersen & Johansson, 2010). Wright & Hornbach (submitted, JGR: Solid Earth) tested the accuracy of Hertz-Mindlin with constraints on all model parameters except coordination number, which they derived from Murphy (1982) 's empirical relationship (Figure 2). They showed that Hertz-Mindlin accurately predicts seismic velocities for vadose sands older than ninety-five years but overpredicts velocities for vadose sands younger than forty-three years. The enigmatic results from these field, numerical, and theoretical studies are an impetus for additional studies of the effectiveness of the other six rock physics models and the influences of microscale grain processes on the models' seismic velocity predictions.

This study assesses the accuracies of the seven abovementioned rock physics models. We discuss the sediment property insights that can be gained from model tests and the best ways to improve and use the models for critical zone studies. Our study area consists of nearly pure vadose zone sand at four sites at Port Royal Beach, Jamaica – i.e., the same sands studied by Wright & Hornbach (submitted, JGR: Solid Earth) (Figure 1). These sands are clean (contain <5 % fines), well-rounded, and highly-spherical (Figure 2), which makes them ideal for rock physics model testing. Furthermore, the site has been trenched, cored, and surveyed with a seismic refraction study so that the greatest uncertainties in physical properties are minimized.

The results show that Jenkins, followed by Walton and Hertz-Mindlin, most accurately predict measured seismic velocities in this study area. We conclude that predictions from these models will further improve when effects of the existence, locations, and strengths of force-chain links are accounted for in the models. Currently, there remains a significant risk of using rock physics models to infer that seismic velocity changes are related to changes to porosity, water saturation, and pore space cement, when instead, the observed velocity changes are caused by changes to grain-contact force distribution.

2 Background

The rock physics models approximate sand as a collection of randomly organized identical spheres subjected to Hertzian contact forces (Hertz, 1881). In the same sand (i.e., same porosity, lithology, and effective stress), differences between model predictions solely arise from how the models treat cementation, grain friction, grain size, and slip at grain contacts (Mindlin, 1949; Digby, 1981; Walton, 1987; Dvorkin & Nur, 1996; Jenkins et al., 2005). We discuss these differences below.

Hertz-Mindlin, Walton, Jenkins, and Digby assume that sands are cementless (Mindlin, 1949; Digby, 1981; Walton, 1987; Jenkins et al., 2005). Contact cement, soft sand, and stiff sand are modified versions of Hertz-Mindlin with the caveat that cement is present within the sand's matrix, reduces porosity, and/or increases grain-grain adhesion (Dvorkin & Nur, 1996). Contact cement assumes that cement is only present at contacts or surrounds the grains (Dvorkin & Nur, 1996). Soft and stiff sand models assume that cement is deposited on the surface of the grains, away from grain contacts (Dvorkin & Nur, 1996). Soft and stiff sand also respectively assume that grains are organized in the weakest and strongest possible configurations, as constrained by the Hashin-Shtrikman bounds (Hashin & Shtrikman, 1963).

The models differ based on assumptions for if, how, and why seismic waves induce microscale grain-contact slip. Hertz-Mindlin, and by extension stiff sand, soft sand, and contact cement, assume that slip occurs after the tangential stresses exceed interparticle grain-contact normal forces (Mindlin, 1949; Dvorkin & Nur, 1996). Walton assumes that normal and tangential slip co-occurs (Walton, 1987). Jenkins approaches slip from a force balance perspective, arguing that grain-contact slip is nonlinear and depends on the force exerted on neighboring grains (Jenkins et al., 2005). Digby assumes that grains are initially bonded across their effective contact radius, and, away from there, grain-contact slip occurs without resistance whenever grain-contact normal forces are exceeded (Digby, 1981). All models (except for Digby) could be modified to assume that grain-contact friction is infinite (rough-grained) or non-existent (smooth-grained) (Mindlin, 1949; Digby, 1981; Walton, 1987; Dvorkin & Nur, 1996; Jenkins et al., 2005). Jenkins and Digby are the only models that parametrize grain size (Digby, 1981; Jenkins et al., 2005). Once all model parameters are constrained, comparisons between modeled and measured velocities could provide insights into which unmeasured model assumptions (e.g., slip mechanism) are poor approximations of real systems and or what additional model parameterizations are needed to represent sands better.

3 Methods

We assess the models' accuracies by comparing modeled versus measured seismic velocities at study sites 1-4 at Port Royal Beach (see Figure 1). Modeling Vp and Vs require constraints on bulk density ρ_b, effective bulk modulus K_{eff} and effective shear modulus μ_{eff}(equations 1-2). Rock physics models and Gassmann-Biot theory provide constraints on K_{eff} and μ_{eff}, whereas ρ_b derives from sidewall cores (Wright & Hornbach, submitted, JGR: Solid Earth).

$$Vp = \sqrt{\frac{\frac{4}{3}\ K_{eff} + \ \mu_{eff}}{\rho_b}} \tag{1}$$

$$Vs = \sqrt{\frac{\mu_{eff}}{\rho_b}} \tag{2}$$

The rock physics equations for the dry-frame elastic moduli are in the appendix. For each model, we constrain:

(A) porosity ϕ using sidewall cores (Wright & Hornbach, submitted, JGR: Solid Earth),

(B) effective hydrostatic pressure P_{eff} using equation 3, where g, W_d, S_w, and Y_w respectively represent gravitational acceleration, water table depth, fluid saturation percentage, and unit weight of water,

$$P_{eff} = \ g\int_0^z \rho_b(z)\ dz\ -[z - W_d]S_w Y_w \tag{3}$$

(C) mineral bulk K_m and shear μ_m moduli using the Hashin-Shtrikman bounds (equations 4-5), where K_f, K_s, μ_f, and μ_s represent fluid bulk modulus, mineral bulk modulus, fluid shear modulus, and mineral shear modulus (Hashin & Shtrikman, 1963),

$$K_m = K_s + \frac{\phi}{\left(K_f - K_s\right)^{-1} + (1-\phi)(K_s + \frac{4}{3}\mu_s)^{-1}} \tag{4}$$

$$\mu_m = \mu_s + \frac{\phi}{\left(\mu_f - \mu_s\right)^{-1} + \frac{2(1-\phi)(K_s + 2\mu_s)}{5\mu_s\left(K_s + \frac{4}{3}\mu_s\right)}} \tag{5}$$

(D) Voigt M_v and Reuss M_R bounds for k_m and μ_m using equation 6-7, where f_i represents the fractional proportion of the elastic moduli m_i of the i^{th} mineral (Hill, 1952),

$$M_v = \sum_{i=1}^{N} f_i m_i \tag{6}$$

$$\frac{1}{M_R} = \sum_{i=1}^{N} \frac{f_i}{m_i} \tag{7}$$

(E) mineral Poison's ratio η_m using equation 8,

$$\eta_m = \frac{3k_m - 2\mu_m}{6k_m + 2\mu_m} \tag{8}$$

(F) and coordination number c using equation 9 (Murphy, 1982).

$$c = 20 - 34\phi + 14\phi^2 \tag{9}$$

We use Gassmann-Biot's formula (equation 10) to estimate the effects of fluid saturation on dry-frame bulk moduli K_{dry} estimated from rock physics models (Gassmann, 1951; Biot, 1956). There, K_{air} and K_{f2} represent the bulk modulus of air at constant temperature (101 kPa) and the bulk modulus of the fluid (i.e., seawater, 2.3 GPa), respectively.

$$\frac{K_{eff}}{K_m - K_{eff}} - \frac{K_{f2}}{\phi(K_m - K_{f2})} = \frac{K_{dry}}{K_m - K_{dry}} + \frac{K_{air}}{\phi(K_m - K_{air})} \tag{10}$$

With K_{eff} constrained, we use equations 1-2 to predict seismic velocities under three scenarios that investigate the models' uncertainties. In scenario one, we empirically constrain coordination numbers with Murphy (1982) 's relationship (equation 9) and predict velocities 10,000 times, each time inputting different groups of model parameters that we randomly select from a uniform distribution of numbers within each parameter's numerical range. This method ensures that uncertainties associated with the measured input model parameters and effective medium bounds (e.g., Hashin-Shtrikman and Voigt-Reuss) are reflected within seismic velocities predictions. In scenario two, we constrain uncertainties in the same way, assume that Murphy (1982) 's coordination number relationship may be erroneous, and instead calculate the coordination number required to best predict seismic velocities. In scenario three, we predict seismic velocities assuming average sand properties (i.e., 100% quartz, $\emptyset_z$ = 0.4, ρ_b = 1.5 g/cm^3, and mineral elastic moduli estimated from Voigt and Reuss bound averages). This scenario assesses the importance of ground-truthing models with in-situ sediment property measurements.

4 Results

Misfits between modeled and predicted seismic velocities vary between the three modeled scenarios, depth, and age (Figure 3-4). Models that use Murphy (1982) 's relationships for coordination number and Monte-Carlo uncertainty analyses (i.e., scenario one models) overpredict seismic velocities at sites 1-2 below ~0.1 cm; misfits are lower for sites 3-4, with the soft sand and all cementless models except Digby accurately predicting seismic velocities. For scenario 2, we find that unrealistically low coordination numbers (1-2) are needed to predict seismic velocities at sites 1-2, whereas the higher predictions from Murphy (1982) 's relationship (4-8) are sufficient to predict velocities at sites 3-4, especially below 1 m depth (Figure 3-4).

Models assuming average sand properties (i.e., scenario three models) generally result in mispredictions; these models perform best for sands deeper than 1 m at site 3.

Regardless of the scenarios, misfits for *Vp* (Figure 3-4) are generally lower than for *Vs* (Figure 3-4). Smooth-grained and cementless models also generally result in lower misfits. Of the cementless models, Jenkins, followed by Walton, Hertz-Mindlin, and Digby, has the lowest mispredictions for *Vp* shallower than 1 m and all depths in *Vs*. Walton, followed by Hertz-Mindlin, Jenkins, and Digby, has the lowest mispredictions for *Vp* beneath 1 m. Of the cement models, the soft sand, followed by the stiff sand and contact cement, results in the lowest misfits. Soft sand is the only cement model that accurately predicts seismic velocities in sections of the sand column with measured cement – i.e., between 0.8-2 m at site 3-4 under scenario one and all depths at sites 1-2 under scenario two.

5 Discussion

Below, we use the results to discuss the significance of misfits between modeled and measured velocities, how to improve the models, and best practices for using the models for critical zone studies. We conclude that the models remain non-unique primarily because of a lack of understanding of how grain-contact forces are distributed.

5.1 Significance of misfits between modeled and predicted seismic velocities

Model comparisons provide insights into grain microstructure. Observations that (1) the models' accuracies improve with age without significant changes to the measured sand properties, (2) cement models more substantially overpredict velocities than cementless ones, and (3) that an unrealistically low coordination number [1-2 versus 4-8 as predicted by Murphy (1982) 's relationship] is needed to predict velocities in younger sands are instructive. The observations further support Wright & Hornbach (submitted, JGR: Solid Earth) 's interpretation that the main difference between sites 1-2 and 3-4 is likely an unmeasured physical property relating to how grains and grain contact forces are distributed within the sand columns. One interpretation to test is whether coordination numbers are similar across all sites [i.e., 4-8 as predicted by Murphy (1982)'s relationship] but seismic velocities are greater in older sands because the younger sands have less load-bearing grains (e.g., 1-3 of the 4-8 that are in contact) that significantly participate in the transmission of seismic waves. Under these conditions, it is not surprising that the lower coordination numbers produce better fits to the measured seismic velocities. The above scenario highlights one of the major drawbacks of using rock physics to study natural shallows sands – i.e., the models treat grains and grain-contact forces as being identical even though these properties are almost certainly not identical.

The model comparisons provide insights into the micro-slip behaviors of vadose zone sands. Observations that smooth-grained models perform better than rough-grained models imply that propagating seismic waves induce microscale elastic grain-contact slip in these sands. Observations that Jenkins generally performs best for scenario one models suggest that a nonlinear grain-contact slip modeling approach may be best, especially in high porosity sands (like we study) where tangential grain-contact slips can more freely occur. Jenkins, Hertz-Mindlin, and Walton do, however, predict velocities similarly (within 5 %) at sites 3-4, implying that other factors are at play (e.g., grain-contact force distribution) and/or slip mechanism is of second-order importance to seismic velocity predictions in the older sands. The most straightforward interpretation is, therefore, that Port Royal Beach sands are generally susceptible to deformation (i.e., grain-contact slippage) during seismic wave propagation (including earthquakes) and that the sands could increase grain-contact forces via grain reorganizing processes such as compaction or contact creep.

The model comparison results suggest that cement most likely reduces porosity and is unlikely to be present at grain contacts. When parameterized with cement fraction estimates (i.e., between 0-3%; Figure 2), lower misfits by the soft sand (versus stiff sand and contact cement) models (Figure 4) are consistent with an interpretation that the grains more probably arrange in the softest configurations as well as that cement is most likely deposited on the grains, but away from contacts. Observations that contact cement and stiff sand overpredict velocities by at least ~500-1000 m/s in most cemented sections of the sand columns also imply that it is unlikely that cement surrounds the grain and/or act as a grain adhesive. Moreover, better predictions by Digby versus contact cement may suggest that any existing grain-grain adhesion (by cement or capillary forces) is likely weaker than stresses induced by seismic wave propagation. Cement, therefore, is unlikely to be the primary controlling factor for changes in seismic velocities with sediment age.

5.2 Improvements needed for better rock physics modeling of the critical zone

Based on these observations, we suggest that rock physics models will most significantly improve with a better understanding of how sands distribute overburden stresses (Makse et al., 1999; Makse et al., 2004; Majmudar & Behringer, 2005; Bachrach & Avseth, 2008). The need for improved understanding of grain-contact force distribution is evidenced by observations that modeled misfits primarily change as a function of coordination number, age, and depth, as opposed to slipping mechanism or grain-contact friction (Figure 3-4). Previous studies' observations that (1) overburden stresses within photoelastic beads become more uniformly distributed (along grain force chain links) with increasing effective pressures (Majmudar & Behringer, 2005), (2) sorting and angularity induced nonuniform grain-contact geometries can cause Hertz-Mindlin to overpredict seismic velocities at 400-600 m depths (Bachrach & Avseth, 2008), and (3) beach, river, and dune sand porosities remain constant down to 17 m are instructive. This, combined with results presented here, supports the hypothesis that, apart from fluid saturation in *Vp*, changes to the seismic velocities of clean critical zone (upper 17 m) sands are primarily controlled by variations in grain-contact force distributions as opposed to grain contact number or porosity reduction alone. If true, we predict that there exists a transition zone or set of conditions, whereby force distribution becomes homogenized within natural sands, and rock physics models become appropriate for use. Testing these predictions will require directly quantifying relationships between coordination number, porosity, sorting, angularity, effective pressure, and force chain-link development within various critical zone depositional environments, preferentially where seismicity is low.

5.3 Implementing rock physics models in future critical zone studies

Results and interpretations from this study highlight the major sources of non-uniqueness in rock physics model solutions. Incorrect model inferences would have likely occurred at one or more of the study sites if we did not constrain all input model parameters (as is often done), used empirically derived coordination number relationships, model velocities with Hertz-Mindlin alone, assume average sand properties, and or did not account for all uncertainties in physical properties and measured seismic velocities. Moreover, the models' relatively poor representations of how overburden stresses are distributed in sands may lead scientists to erroneously associate grain microstructure-induced seismic velocity changes to changes in porosity, water saturation, and/or pore space cement. Along with modifying the models to account for force-chain distribution better, we recommend that future studies use direct measurements to ground-truth and identify which models best predict seismic velocities at multiple locations within each new critical zone environment. Future studies should also explore the wide range of potential uncertainties discussed within this and other studies (e.g., Maske, 1999; Bachrach & Avseth, 2008).

6 Conclusions

Given the increasing use of rock physics models to explain changes to seismic velocities within the critical zone, it is prudent that the community explores the effectiveness of rock physics models, understand their limitations, and improve them where necessary. On this backdrop, this paper discusses if, how, and under what conditions should critical zone scientists use rock physics models to characterize the physical properties of sands, fluids, and cement within the vadose zone and possibly down to at least 17 m. In their current form, each model overpredicts seismic velocities for vadose sands younger than forty-three years. Their accuracies improve for vadose sands older than ninety-four years, which we interpret to be the result of microscale grain re-organizations that lead to a more uniform distribution of grain-contact forces with time Jenkins, followed by Walton, Hertz-Mindlin, and soft sand results in the lowest mispredictions. When combined with other studies, our results suggest that these rock physics models will most substantially improve when they are modified to account for changes to the existence, locations, and strengths of grain-grain force chain links as a function of age and effective pressure. Until then, care should be taken when using rock physics models to study critical zone sands – i.e., all uncertainties should be explored, and the models should be ground-truth in each new study area.

7 Acknowledgements

Thanks to J. Lorenzo and M. Manga for constructive feedback during manuscript preparation. This work was partially funded by a Society of Exploration Geophysicists

Geoscientists without Borders grant provided to Matt Hornbach and by the SMU Institute for Science, Earth, and Man grant to Vanshan Wright.

References

Andersen, C. F., & Johansen, T. A. (2010). Test of rock physics models for prediction of seismic velocities in shallow unconsolidated sands: A well log data case. *Geophysical Prospecting*. doi:10.1111/j.1365-2478.2010.00870.x

Anderson, S. P., Blanckenburg, F. V., & White, A. F. (2007). Physical and Chemical Controls on the Critical Zone. *Elements, 3*(5), 315-319. doi:10.2113/gselements.3.5.315

Atkins, J., & McBride, E. (1992). Porosity and Packing of Holocene River, Dune, and Beach Sands. *AAPG Bulletin, 76*. doi:10.1306/bdff87f4-1718-11d7-8645000102c1865d

Bachrach, R., & Avseth, P. (2008). Rock physics modeling of unconsolidated sands: Accounting for nonuniform contacts and heterogeneous stress fields in the effective media approximation with applications to hydrocarbon exploration. *Geophysics, 73*(6). doi:10.1190/1.2985821

Bachrach, R., Dvorkin, J., & Nur, A. M. (2000). Seismic velocities and Poisson's ratio of shallow unconsolidated sands. *Geophysics, 65*(2), 559-564. doi:10.1190/1.1444751

Biot, M. A. (1956). Theory of Propagation of Elastic Waves in a Fluid-Saturated Porous Solid. II. Higher Frequency Range. *The Journal of the Acoustical Society of America, 28*(2), 179-191. doi:10.1121/1.1908241

Day-Lewis, F. D. (2005). Applying petrophysical models to radar travel time and electrical resistivity tomograms: Resolution-dependent limitations. *Journal of Geophysical Research, 110*(B8). doi:10.1029/2004jb003569

Digby, P. J. (1981). The Effective Elastic Moduli of Porous Granular Rocks. *Journal of Applied Mechanics, 48*(4), 803-808. doi:10.1115/1.3157738

Dvorkin, J., & Nur, A. (1996). Elasticity of high-porosity sandstones: Theory for two North Sea data sets. *Geophysics, 61*(5), 1363-1370. doi:10.1190/1.1444059

Flinchum, B. A., Holbrook, W. S., Grana, D., Parsekian, A. D., Carr, B. J., Hayes, J. L., & Jiao, J. (2018). Estimating the water holding capacity of the critical zone using near-surface geophysics. *Hydrological Processes, 32*(22), 3308-3326. doi:10.1002/hyp.13260

Gassmann, F. (1951). Uber di elastizitat poroser median. *Vier. Der Natur Gesellschaft in Zurich, 96*, 1-23.

Hashin, Z., & Shtrikman, S. (1963). A variational approach to the theory of the elastic behaviour of multiphase materials. *Journal of the Mechanics and Physics of Solids, 11*(2), 127-140. doi:10.1016/0022-5096(63)90060-7

Hertz, H. (1881). On the contact of elastic solids. *Z. Reine Angew. Mathematik,* (92), 156-171.

Hill, R. (1952). The Elastic Behaviour of a Crystalline Aggregate. *Proceedings of the Physical Society. Section A, 65*(5), 349-354. doi:10.1088/0370-1298/65/5/307

Holbrook, W. S., Riebe, C. S., Elwaseif, M., Hayes, J. L., Basler-Reeder, K., Harry, D. L., . . . Hopmans, J. W. (2014). Geophysical constraints on deep weathering and water storage potential in the Southern Sierra Critical Zone Observatory. *Earth Surface Processes and Landforms, 39*(3), 366-380. doi:10.1002/esp.3502

Jenkins, J. (2005). Fluctuations and the effective moduli of an isotropic, random aggregate of identical, frictionless spheres. *Journal of the Mechanics and Physics of Solids, 53*(1), 197-225. doi:10.1016/j.jmps.2004.06.002

Majmudar, T. S., & Behringer, R. P. (2005). Contact force measurements and stress-induced anisotropy in granular materials. *Nature, 435*(7045), 1079-1082. doi:10.1038/nature03805

Makse, H. A., Gland, N., Johnson, D. L., & Schwartz, L. (2004). Granular packings: Nonlinear elasticity, sound propagation, and collective relaxation dynamics. *Physical Review E, 70*(6). doi:10.1103/physreve.70.061302

Makse, H. A., Gland, N., Johnson, D. L., & Schwartz, L. M. (1999). Why Effective Medium Theory Fails in Granular Materials. *Physical Review Letters, 83*(24), 5070-5073. doi:10.1103/physrevlett.83.5070

Mavko, G., Mukerji, T., & Dvorkin, J. (2020). The Rock Physics Handbook. doi:10.1017/cbo9780511626753

Mindlin, R. D. (1949). Compliance of elastic bodies in contact. *Journal of Applied Mechanics, 16*, 259-268.

Mota, L. (1954). Determination Of Dips And Depths Of Geological Layers By The Seismic Refraction Method. *Geophysics, 19*(2), 242-254. doi:10.1190/1.1437988

Murphy, W. F. (1982). *Effects of microstructure and pore fluids on the acoustic properties of granular sedimentary materials* (Unpublished doctoral dissertation). Stanford University.

Parsekian, A. D., Singha, K., Minsley, B. J., Holbrook, W. S., & Slater, L. (2015). Multiscale geophysical imaging of the critical zone. *Reviews of Geophysics, 53*(1), 1-26. doi:10.1002/2014rg000465

Rabbel, W. (2009). Seismic methods (R. Kirsch, Ed.). In *Groundwater geophysics: A tool for hydrogeology* (pp. 23-84). Berlin: Springer. doi:doi:10.1007/978-3-540-88405-7

Rodell, M., Chen, J., Kato, H., Famiglietti, J. S., Nigro, J., & Wilson, C. R. (2006). Estimating groundwater storage changes in the Mississippi River basin (USA) using GRACE. *Hydrogeology Journal, 15*(1), 159-166. doi:10.1007/s10040-006-0103-7

Selker, J. S., Thévenaz, L., Huwald, H., Mallet, A., Luxemburg, W., Giesen, N. V., . . . Parlange, M. B. (2006). Distributed fiber-optic temperature sensing for hydrologic systems. *Water Resources Research, 42*(12). doi:10.1029/2006wr005326

Shen, J., Crane, J. M., Lorenzo, J. M., & White, C. D. (2016). Seismic velocity prediction in shallow (< 30 m) partially saturated, unconsolidated sediments using effective medium theory. *Journal of Environmental and Engineering Geophysics*, 21(2), 67-78. doi: 10.2113/jeeg21.2.67

Stephenson, W. J. (2005). Blind Shear-Wave Velocity Comparison of ReMi and MASW Results with Boreholes to 200 m in Santa Clara Valley: Implications for Earthquake Ground-Motion Assessment. *Bulletin of the Seismological Society of America, 95*(6), 2506-2516. doi:10.1785/0120040240

Walton, K. (1987). The effective elastic moduli of a random packing of spheres. *Journal of the Mechanics and Physics of Solids, 35*(2), 213-226. doi:10.1016/0022-5096(87)90036-6

Watt, J. P., Davies, G. F., & O'connell, R. J. (1988). The elastic properties of composite materials. *Elastic Properties and Equations of State,* 384-406. doi:10.1029/sp026p0384

Wright, V., & Hornbach, M. (submitted). The effects of 180 years of aging on the physical properties of partially saturated sands. *Journal of Geophysical Research: Solid Earth*.

FIGURE CAPTIONS

Figure 1. (A) Map [adapted from Wright & Hornbach (submitted, JGR: Solid Earth)] shows Kington Jamaica. The red box highlights Port Royal, a town on the eastern terminus of a complex sand spit. (B-C) Aerial images [also adapted from Wright & Hornbach (submitted, JGR: Solid Earth)] show Port Royal Beach, the locations of beach's past shoreline positions, and sites of refraction surveys and sediment sampling. The sands' ages [i.e., 1988-2016, 1956-1974, 1909-1923, and 1837-1862 at sites 1-4, respectively] derive from legacy maps of Port Royal (Wright & Hornbach, submitted, JGR: Solid Earth).

Figure 2. (A-J) Graphs [adapted from Wright & Hornbach (submitted, JGR: Solid Earth)] show sediment physical properties results, which we use as inputs into the rock physics models. These sediment physical properties derive from sidewall sediment coring analyses (Wright & Hornbach, submitted, JGR: Solid Earth).

Figure 3. Comparisons between measured and modeled seismic velocities for all four sites. Note that the Jenkins produces imaginary solutions if coordination numbers are between 1-2 at Port Royal Beach. The measured compressional wave velocities derive from the first-break geometric and tau-p methods for estimating seismic velocities from refraction survey shot gathers; first-break were picked by nine geophysicists (including the first author) and randomized (as a function of geophone position) to create 100 different travel time curves used to create the seismic velocity-depth profiles (Wright & Hornbach, submitted, JGR: Solid Earth). The shear wave velocities derive from multichannel analyses of surface wave (MASW), with the selected

models being the 100 that have the lowest Akaike Information Criterion scores (Wright & Hornbach, submitted, JGR: Solid Earth).

Figure 4. Comparisons between measured and modeled shear wave seismic velocities for all four sites and models. Note that for model scenarios one and three, the contact-cement model predicts that the *Vs* and *Vp* greater than 850 m/s for all depths. The caption for figure 3 explains the methods used to calculate measured seismic velocities.

Figure 1.

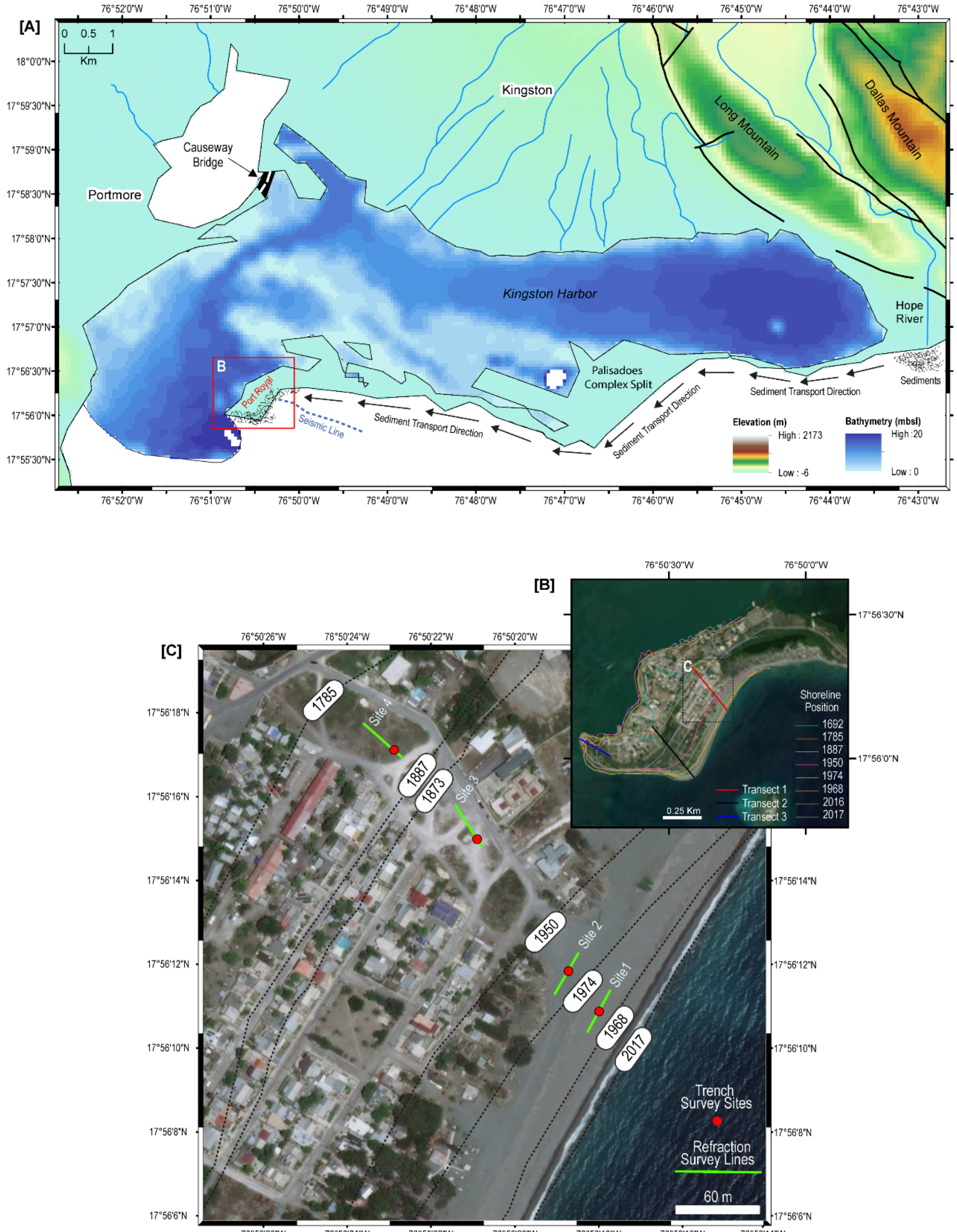
[A]
Kingston
Causeway Bridge
Portmore
Long Mountain
Dallas Mountain
Kingston Harbor
Hope River
Palisadoes Complex Split
Port Royal
Seismic Line
Sediment Transport Direction
Sediments
Elevation (m)
High : 2173
Low : -6
Bathymetry (mbsl)
High :20
Low : 0
[B]
Shoreline Position
1692
1785
1887
1950
1974
1968
2016
2017
Transect 1
Transect 2
Transect 3
0.25 Km
[C]
1785
1887
1873
1950
1974
1968
2017
Site 1
Site 2
Site 3
Site 4
Trench Survey Sites
Refraction Survey Lines
60 m

Figure 2.

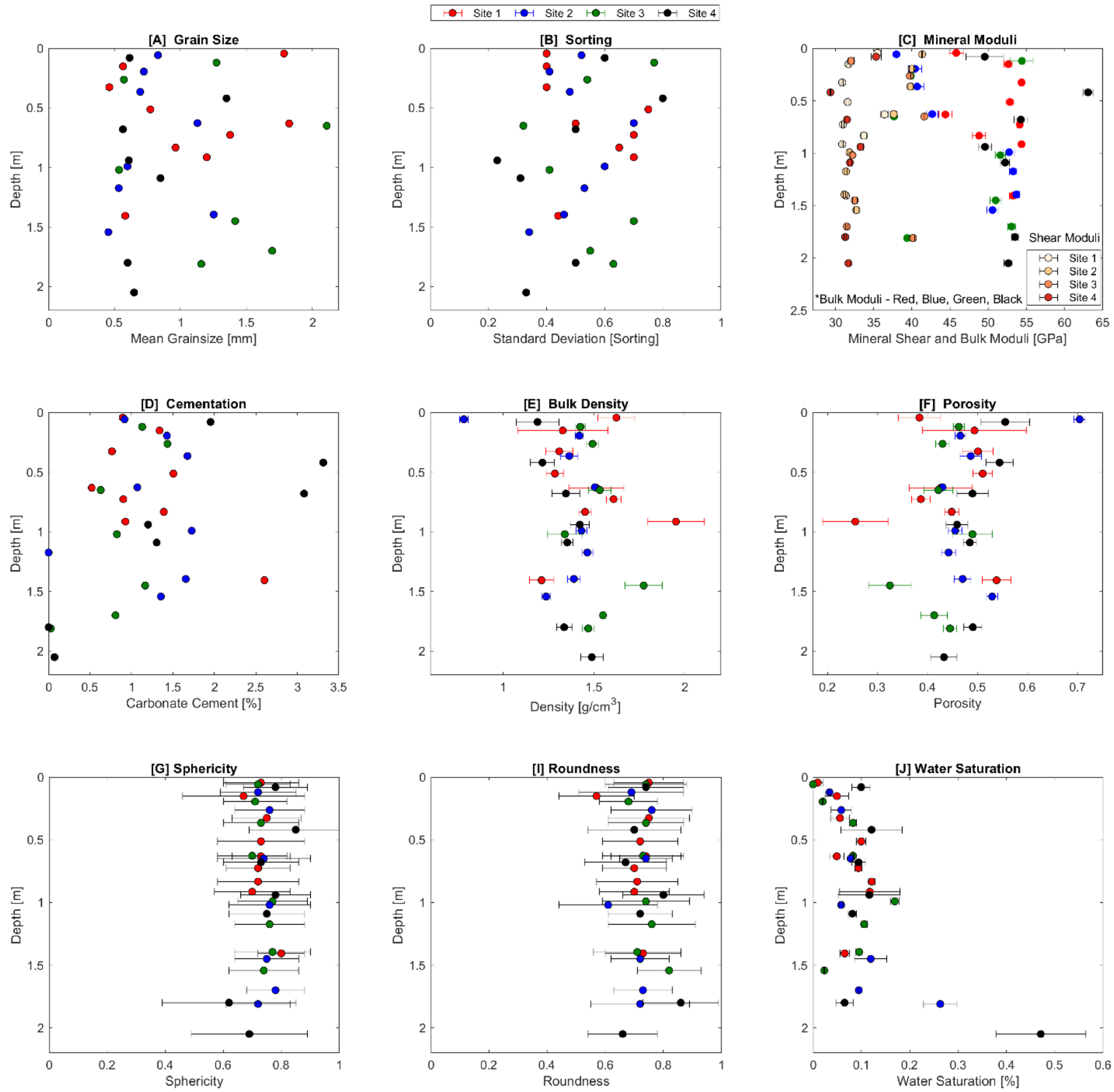
Site 1
Site 2
Site 3
Site 4
[A] Grain Size
Depth [m]
Mean Grainsize [mm]
[B] Sorting
Standard Deviation [Sorting]
[C] Mineral Moduli
Shear Moduli
*Bulk Moduli - Red, Blue, Green, Black
Mineral Shear and Bulk Moduli [GPa]
[D] Cementation
Carbonate Cement [%]
[E] Bulk Density
Density [g/cm3]
[F] Porosity
Porosity
[G] Sphericity
Sphericity
[I] Roundness
Roundness
[J] Water Saturation
Water Saturation [%]

Figure 3.

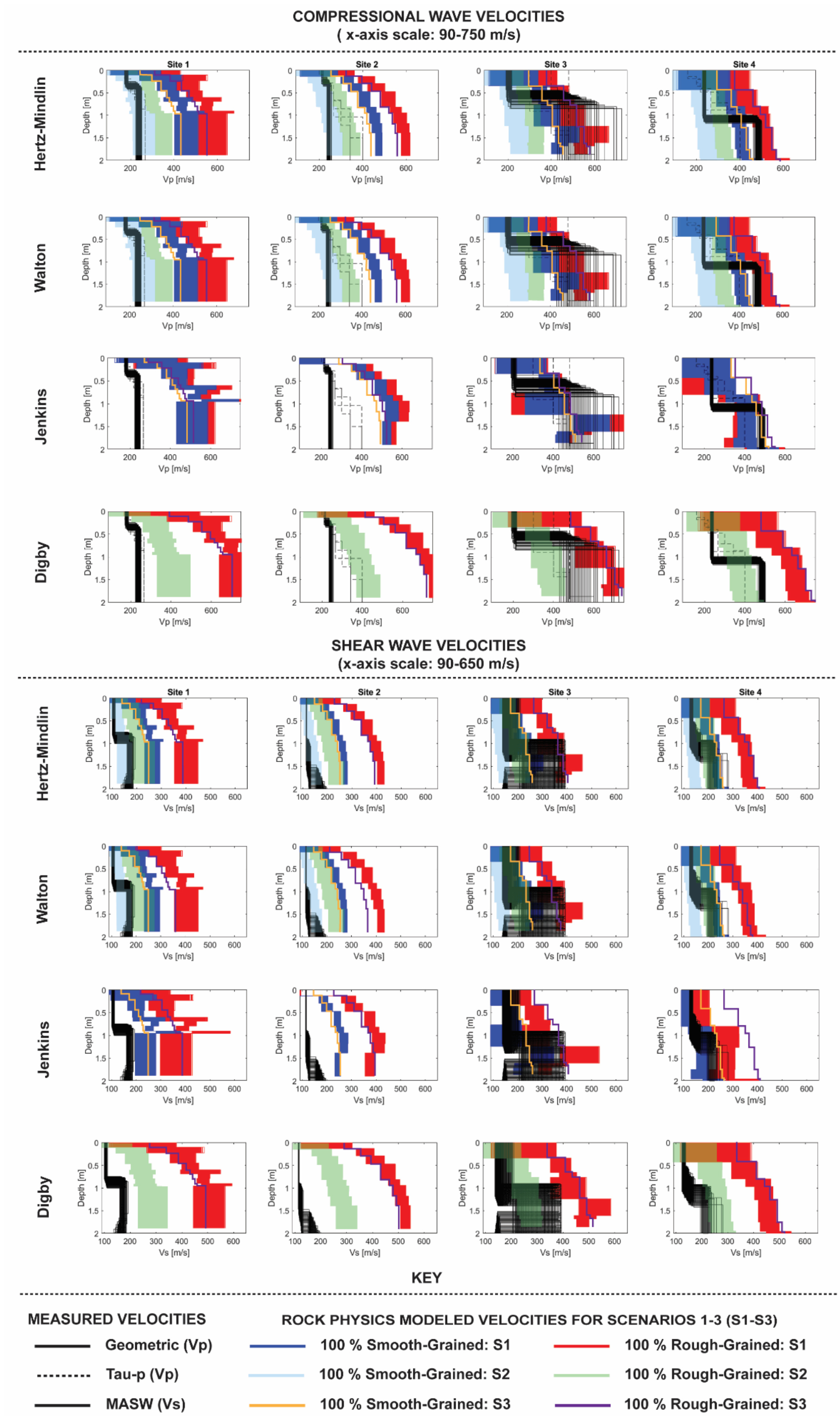
COMPRESSIONAL WAVE VELOCITIES
(x-axis scale: 90-750 m/s)
Site 1
Site 2
Site 3
Site 4
Hertz-Mindlin
Walton
Jenkins
Digby
Depth [m]
Vp [m/s]
SHEAR WAVE VELOCITIES
(x-axis scale: 90-650 m/s)
Vs [m/s]
KEY
MEASURED VELOCITIES
Geometric (Vp)
Tau-p (Vp)
MASW (Vs)
ROCK PHYSICS MODELED VELOCITIES FOR SCENARIOS 1-3 (S1-S3)
100 % Smooth-Grained: S1
100 % Smooth-Grained: S2
100 % Smooth-Grained: S3
100 % Rough-Grained: S1
100 % Rough-Grained: S2
100 % Rough-Grained: S3

Figure 4.

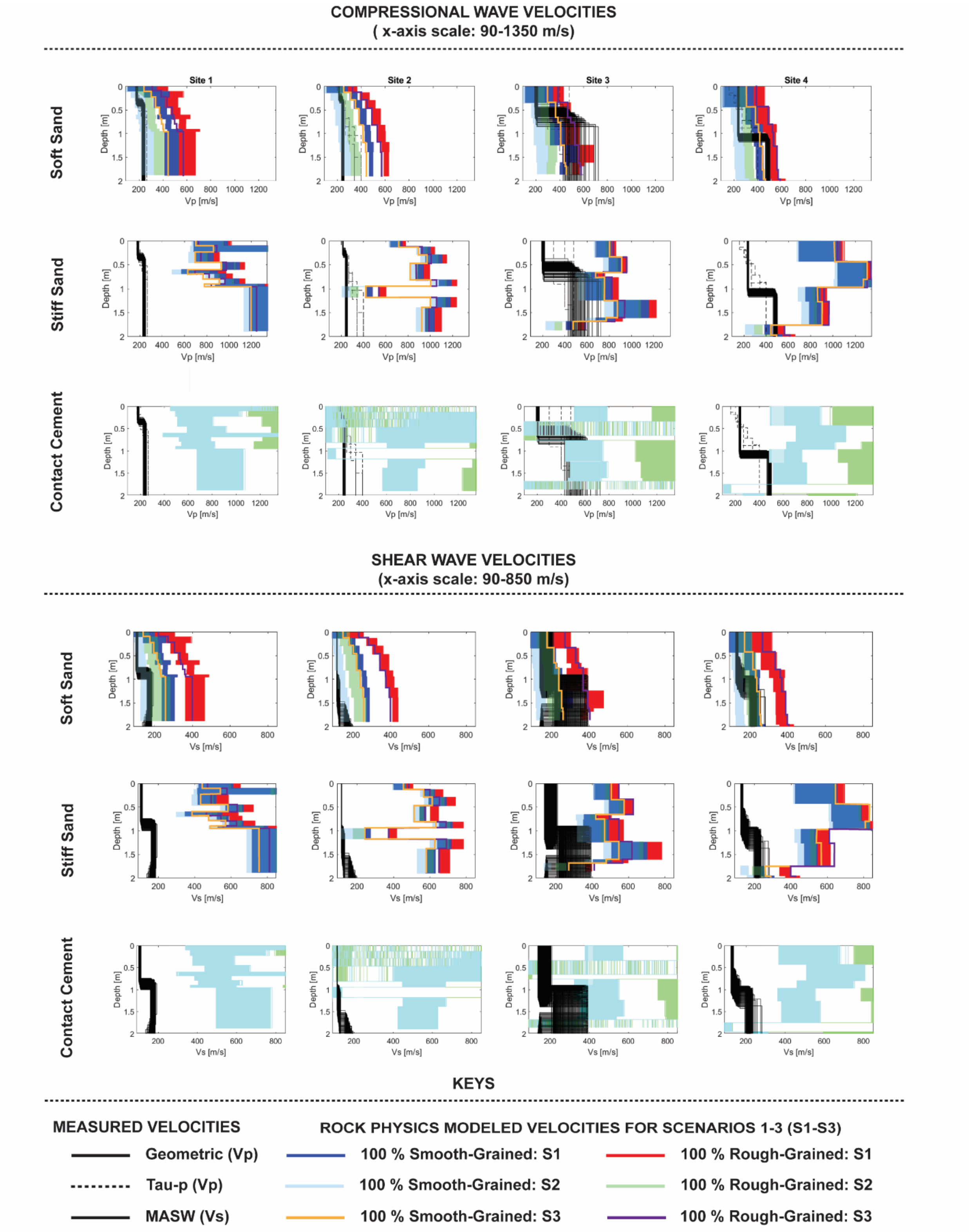
COMPRESSIONAL WAVE VELOCITIES
(x-axis scale: 90-1350 m/s)
Site 1
Site 2
Site 3
Site 4
Soft Sand
Stiff Sand
Contact Cement
Depth [m]
Vp [m/s]
SHEAR WAVE VELOCITIES
(x-axis scale: 90-850 m/s)
Vs [m/s]
KEYS
MEASURED VELOCITIES
Geometric (Vp)
Tau-p (Vp)
MASW (Vs)
ROCK PHYSICS MODELED VELOCITIES FOR SCENARIOS 1-3 (S1-S3)
100 % Smooth-Grained: S1
100 % Smooth-Grained: S2
100 % Smooth-Grained: S3
100 % Rough-Grained: S1
100 % Rough-Grained: S2
100 % Rough-Grained: S3

APPENDIX

This appendix lists the equations for the dry-frame elastic moduli for each rock physics model. We refer the interested readers to the original papers for derivations of each equation and Mavko (2020) for briefer descriptions of the models' equations.

Nomenclature

K_{dry} – dry-frame bulk modulus

μ_{eff} – shear modulus (note: μ_{dry} = μ_{eff} under hydrostatic pressure conditions)

ϕ – measured porosity

P_{eff} – effective hydrostatic pressure

K_m – bulk modulus

μ_m – shear modulus

η_m – mineral Poison's ratio

c – coordination number

f – volume from of rough versus smooth grains (note: f = 1 for 100 % rough grains)

R – average grain radius

K_{hm} – dry-frame bulk modulus from Hertz-Mindlin

μ_{hm} – dry-frame shear modulus result from Hertz-Mindlin

ξ – cement fraction

ϕ_c – critical porosity

K_c – bulk moduli of the cement

μ_c – shear moduli of the cement

η_c – Poisson's ratio of the measured cement

Hertz-Mindlin

$$K_{dry} = \left[\frac{(1-\emptyset)^2 c^2 \mu_m^2 P_{eff}}{18\pi^2(1-\eta_m)^2)}\right]^{\frac{1}{3}}$$

$$\mu_{eff} = \frac{2+3f-\eta_m(1+3f)}{5(2-\eta_m)}\left[\frac{3(1-\emptyset)^2 c^2 \mu_m^2 P_{eff}}{2\pi^2(1-\eta_m)^2}\right]$$

Walton

100 % rough-grained model

$$K_{dry} = \frac{1}{6}\left[\frac{3(1-\emptyset)^2 c^2 P_{eff}}{\pi^4 B^2}\right]^{\frac{1}{3}}$$

$$\mu_{eff} = \frac{3}{5} K_{\ eff} \frac{5B + A}{2B + A}$$

100 % smooth-grained model

$$K_{dry} = \frac{1}{10}\left[\frac{3(1-\emptyset)^2 c^2 P_{eff}}{\pi^4 B^2}\right]^{\frac{1}{3}}$$

$$\mu_{\ eff} = \frac{3}{5} K_{eff}$$

where

$$A = \frac{1}{4\pi}\left(\frac{1}{\mu_m} - \frac{1}{\mu_m + \lambda}\right)$$

$$B = \frac{1}{4\pi}\left(\frac{1}{\mu_m} + \frac{1}{\mu_m + \lambda}\right)$$

$$\lambda = k_m$$

$$-\frac{2}{3}\mu_m$$

Jenkins

$$\mu_{eff} = \left[\left(\frac{K_n c(1-\phi)}{5\pi R^2}\right)\left(1 - 2(w_1 + 2w_2)\right)\left(\frac{c}{3}\right)^{-1}\right] - \left[(K_1 + 2K_2)\left(\frac{c}{3}\right)^{-2}\right]$$

$$+ \left[(e_1 + 2e_2)\left(\frac{c}{3}\right)^{-3}\left(\frac{2-\eta_m + 3f(1-\eta_m)}{2-\eta_m}\right)\right]$$

$$K_{dry} = \frac{2}{3}\mu_{eff} + \left[\left(\frac{K_n c(1-\phi)}{5\pi R^2}\right)\ (1 - 2\left(\frac{c}{3}\right)^{-1})\ (w_1 + 7w_2)\right]$$

$$+ \left[2(K_1 + 2K_2 + 5K_3)\ \left(\frac{c}{3}\right)^{-2}\right]$$

$$- \left[(e_1 + 2e_2 + 5e_3)2\left(\frac{c}{3}\right)^{-3}\left(\frac{2-\eta_m - 2f(1-\eta_m)}{2-\eta_m}\right)\right]$$

<u>where</u>

$$K_n = \left[\frac{\frac{3\mu_m \pi P_{eff}(1-\phi)}{1-\eta_m}}{2c\mu_m(1-\phi)}\right]^{\frac{1}{3}}$$

$$e_1 = n_1 w_1 + n_2 w_1 + 2n_2 w_2$$

$$e_2 = n_1 w_2$$

$$e_3 = n_2 w_2 + n_1 w_2$$

$$w_1 = \frac{166 - 11c}{128}$$

$$w_2 = -\frac{c + 14}{128}$$

$$n_1 = b_1 - \alpha_1^2$$

$$n_2 = b_2 - (2\alpha_1\alpha_{2'} + \alpha_{2'}^2)$$

$$\alpha_1 = \frac{19c - 22}{48}$$

$$\alpha_{2'} = \frac{18 - 9c}{4}$$

$$b_1 = \psi_1 + \alpha_1$$

$$b_2 = \psi_2 + \alpha_{2'}$$

$$\psi_1 = \frac{1.96(c-2)(c-4) + 3.30\, c\,(c-2) + 0.49c\,(c-4) + 0.32c^2}{16\pi}$$

$$\psi_2 = -\frac{2.16\,(c-2)(c-4) + 2.30c(c-2) + 0.54c(c-4) - 0.06c^2}{16\pi}$$

$$K_1 = a_1 - a_1 w_{1\prime} + w_{1\prime} \alpha_{2\prime} + 2w_2 a \alpha_{2\prime}$$

$$K_2 = a_2 - w_2 \alpha_1$$

$$K_3 = a_3 - w_2 \alpha_{2\prime} + w_2 \alpha_1$$

$$w_{1\prime} = \frac{38 - 11c}{128}$$

$$a_1 = w_{1\prime} + g_1$$

$$a_2 = w_2 + g_2$$

$$a_3 = w_2 + g_3$$

$$g_1 = -\frac{0.52(c-2)(c-4) + 0.10c(c-2) - 0.13c(c-4) - 0.01c^2}{16\pi}$$

$$g_2 = \frac{0.44(c-2)(c-4) - 0.24c(c-2) - 0.11c(c-4) - 0.14c^2}{16\pi}$$

$$g_3 = -\frac{0.44(c-2)(c-4) - 0.42c(c-2) - 0.11c(c-4) + 0.04c^2}{16\pi}$$

Digby

$$K_{dry} \;=\; c(1-\phi)\frac{\dfrac{4\mu_m\left(\sqrt{d^2+\left[\frac{a}{R}\right]^2}\right)}{1-\eta_m}}{12\pi}$$

$$\mu_{eff} = \; c(1-\phi)\frac{\dfrac{4\mu_m\sqrt{d^2+\left[\frac{a}{R}\right]^2}}{1-\eta_m}+\dfrac{\frac{12\mu_m a}{R}}{2-\eta_m}}{20\pi}$$

<u>where</u>

$$a \;=\; \left[\frac{\dfrac{12\pi R^3 P_{eff}}{2c(1-\phi)})}{\dfrac{4}{\frac{1-\eta_m^2}{K_m}+\frac{1-\eta_m^2}{\mu_m}}}\right]^{\frac{1}{3}}$$

$$d^{\,3} \;+\; \frac{3}{2}\left(\frac{a}{R}\right)^2 d \;-\frac{3\pi(1-\eta_m)P_{eff}}{2c(1-\phi)\mu_m} = 0$$

Soft Sand

$$K_{dry} = -\frac{4}{3}\mu_{hm} + \left[\frac{\frac{\phi}{\phi_c}}{K_{hm} + 4\frac{4}{3}\mu_{hm}} + \frac{1 - \frac{\phi}{\phi_c})}{K_m + \frac{4}{3}\mu_{hm}}\right]^{-1}$$

$$\mu_{eff} = -A + \left[\frac{\frac{\phi}{\phi_c}}{\mu_{hm} + A} + \frac{1 - \frac{\phi}{\phi_c}}{\mu_m + A}\right]^{-1}$$

<u>where</u>

$$\phi_c = 1 - \left[(1 - \phi) - (1 - \phi)\frac{\xi}{100}\right]$$

$$A = \frac{\mu_{hm}}{6}\left[\frac{9K_{hm} + 8\,\mu_{hm}}{K_{hm} + 2\mu_{hm}}\right]$$

Stiff Sand Model

$$K_{dry} \;=-\frac{4}{3}\mu_m \;+\; \left[\frac{\frac{\phi}{\phi_c}}{K_{hm}+\frac{4}{3}\mu_m}+\;\frac{1-\frac{\phi}{\phi_c})}{K_m+\frac{4}{3}\mu_m}\right]^{-1}$$

$$\mu_{eff} \;=\; -A \;+\; \left[\frac{\frac{\phi}{\phi_c}}{\mu_{hm}+A}\;+\;\frac{1-\frac{\phi}{\phi_c}}{\mu_m+A}\right]^{-1}$$

<u>where</u>

$$\phi_c =\; 1-\left[(1-\phi)\;\;-\;(1-\phi)\;\frac{\xi}{100}\right]$$

$$A \;=\; \frac{\mu_m}{6}\left[\frac{9K_m+8\,\mu_m}{K_m+2\mu_m}\right]$$

Contact Cement

Cement at grain contacts only

$$K_{dry} = \left(K_c + \frac{4\mu_c}{3}\right)\left(\frac{c(1-\emptyset_c)}{6}\right)(-a_c^2 0.024153\lambda_a^{-1.3646} + a_c 0.20405\lambda_a^{-0.89008} + 0.00024649\lambda_a^{-1.9864})$$

$$\mu_{eff} = K_{eff} + \frac{4}{3}\left[\frac{2}{3}K_{eff} + \left(\frac{3\mu_c c(1-\emptyset_c)}{20}\right)\left(a_c^2 a_{1t}\lambda_\tau^{a_{2t}} + a_c b_{1t}\lambda_\tau^{b_{2t}} + C_{1t}\lambda_\tau^{C_{2t}}\right)\right]$$

Cement surrounds grains

$$K_{dry} = \left(K_c + \frac{4\mu_c}{3}\right)\left(\frac{c(1-\emptyset_c)}{6}\right)(-a_s^2 0.024153\lambda_a^{-1.3646} + a_s 0.20405\lambda_a^{-0.89008} + 0.00024649\lambda_a^{-1.9864})$$

$$\mu_{eff} = K_{eff} + \frac{4}{3}\left[\frac{2}{3}K_{eff} + \left(\frac{3\mu_c c(1-\emptyset_c)}{20}\right)\left(a_s^2 a_{1t}\lambda_\tau^{a_{2t}} + a_s b_{1t}\lambda_\tau^{b_{2t}} + C_{1t}\lambda_\tau^{C_{2t}}\right)\right]$$

where

$$\phi_c = 1 - \left[(1-\phi) - (1-\phi)\,\frac{\xi}{100}\right]$$

$$a_c = 2\sqrt{\frac{(\phi_c - Phi0)}{3c(1-\phi_c)}}^{\frac{1}{4}}$$

$$a_s = \sqrt{\frac{2(\phi_c - Phi0)}{3(1-\phi_c)}}$$

$$\lambda_a = \frac{2\mu_c(1-\eta_m)(1-\eta_c)}{\pi\mu_m(1-2\eta_c)}$$

$$\lambda_\tau = \frac{\mu_c}{\pi\mu_m}$$

$$a_{1t} = -0.01(2.2606{\eta_m}^2 + 2.0696\eta_m + 2.2952)$$

$$a_{2t} = 0.079011{\eta_m}^2 + 0.17539\eta_m - 1.3418$$

$$b_{1t} = 0.05728{\eta_m}^2 + 0.09367\eta_m + 0.20162$$

$$b_{2t} = 0.027425{\eta_m}^2 + 0.052859\eta_m - 0.87653$$

$$C_{1t} = 0.0001(9.6544{\eta_m}^2 + 4.9445\eta_m + 3.1008)$$

$$C_{2t} = 0.018667{\eta_m}^2 + 0.4011\eta_m - 1.8186$$